Indian Journal of Pure & Applied Physics
Vol. 52, August 2014, pp. 550-555

Hydrothermal synthesis of $NiFe_2O_4$, $Ni_{0.6}Zn_{0.4}Fe_2O_4$ and $Ni_{0.6}Zn_{0.4}Fe_2O_4/SrFe_2O_4$: nanostructure, magnetic and dielectric properties

Sukhdeep Singh[1], Manpreet Singh[1], R K Kotnala[2] & Kuldeep Chand Verma[3]*

[1]Akal School of Chemistry, Eternal University, Baru Sahib, Himachal Pradesh 173 101, India

[2]National Physical Laboratory, New Delhi 110 012, India

[3]Akal School of Physics, Eternal University, Baru Sahib, Himachal Pradesh 173 101, India

*E-mail: kuldeep0309@yahoo.co.in ; dkuldep.physics@gmail.com

Received 6 January 2014; revised 6 March 2014; accepted 12 June 2014

$NiFe_2O_4$ (NF), $Ni_{0.6}Zn_{0.4}Fe_2O_4$ (NZF) and $Ni_{0.6}Zn_{0.4}Fe_2O_4/SrFe_2O_4$ (NZF/SF) nanostructures were prepared by hydrothermal synthesis at 180°C/48 h. The synthesis of NF shows nanoparticles of average size 19 nm. However, NZF and NZF/SF show nanowires of average diameter ~23 and 6 nm, and length 325 and 160 nm, respectively. A growth mechanism for fabrication of nanostructure is given. The X-ray diffraction pattern confirms the polycrystalline structure of spinel phase of NF and NZF and orthorhombic phase of SF ferrite. The microstructural analysis is confirmed by transmission electron microscopy. The ferromagnetic behaviour of each ferrite sample is confirmed by *M-H* hysteresis. However, the *M-H* hysteresis of composite NZF/SF also shows spring like vibrations which indicate a strong coupling between hard and soft phases. The higher value of remanent magnetization is observed in NZF/SF which is possible by combining soft/hard ferrite phase. The effect of low dimensions of NZF/SF nanostructure is to control dielectric constant with low loss up to higher frequency of 120 MHz, has been observed.

Keywords: Ferrite, Nanostructures, Hydrothermal synthesis, Magnetism, Dielectric properties

1 Introduction

Magnetism of low-dimensional materials is one of the most attractive current issues because of technological requirements for higher density recording media as well as a fundamental interest in particle size effects on the magnetic properties. One dimensional (1-D) nanostructural ferrites (nanorods, nanowires, nanotubes etc.) become significantly important due to their surface and quantum confinement effects which further, depend on large surface to volume ratio and size dependent properties[1,2], respectively. With optimized external magnetic fields, we should be able to assemble nanorods or nanowires into oriented 1D or 2D arrays, providing a uniform anisotropic magnetic platform for various applications in enhanced data storage, magneto-electron transport[3], etc. The various cubic spinel nanostructures, MFe_2O_4 (M = Fe^{2+}, Mn^{2+}, Co^{2+}, Ni^{2+}, Zn^{2+}, Sr^{2+} etc.) where oxygen forms *fcc* closed packing and M^{2+} and Fe^{3+} occupy either tetrahedral (*A*) or octahedral (*B*) interstitial sites exhibit interesting magnetic properties, high electrical resistivity, mechanical hardness, and chemical stability[4,5]. The M^{2+} occupies only *A* sites in the normal spinel and *B* in an inverse spinel structure; therefore, magnetic properties of MFe_2O_4 ferrite depend on adjustment of the chemical states[6] of M^{2+}.

$NiZnFe_2O_4$ ferrite is a soft magnetic ceramic that has spinel structure based on face centred cubic lattice of the oxygen ions, with the unit cell consisting of 8 formula units $(Zn_xFe_{1-x})[Ni_{1-x}Fe_{1+x}]O_4$ where the ions in ( ) occupy the tetrahedral *A* sites and in [ ] occupy the octahedral[7] *B*. In our previous work, the enhancement in magnetization is observed at room temperature in nickel and nickel zinc ferrite nanoparticles but the dielectric behaviour shows resonance near 10 MHz of frequency[8,9]. Generally, the high resistivity of very small size ferrite nanoparticles results into higher frequency dependent dielectric properties but a superparamagnetic behaviour is the serious disadvantage which lowers its magnetic applications. Therefore, the large surface to volume ratio of ferrite nanostructure (nanorods, nanowires etc.) exhibits unique properties such as spin canting, surface anisotropy, high resistivity etc. which may recover the required limitation of dielectric and magnetic properties.

Recently, the demand for increasing information density and signal-to-noise ratio and allowing writeability, e.g. exchange-coupled composite media,

composite granular continuous media and percolated media[10], a composite of soft/hard ferrite layer proposed excellent properties. It is based on the direct exchange coupling a cross grain boundaries, which make an intimate mixture of nano size grains behave differently from a pure superposition of the grains individual magnetic properties. To get benefit from the coupling, the grain size of the soft phase should not largely exceed the exchange length of the hard magnetic phase. Otherwise, a domain wall can form in the low anisotropic phase at sufficient distance from the hard phase, and the so-initiated magnetization process will easily reverse the whole magnet. To reduce bit size in magnetic recording requires higher uniaxial anisotropy, exchange coupling was proposed to achieve moderate coercivities and thus write fields while maintaining the stability against thermal demagnetization at room temperature[11]. Nanostructures composed of nanowire, nanorods etc. show enhanced magnetic properties due to inter-grain exchange interactions within the exchange correlation length.

In the present paper, we have prepared $NiFe_2O_4$ (NF), $Ni_{0.6}Zn_{0.4}Fe_2O_4$ (NZF) and $Ni_{0.6}Zn_{0.4}Fe_2O_4/SrFe_2O_4$ (NZF/SF) nanostructure by hydrothermal synthesis at 180°C for 48 h. The resulting structural, microstructural, dielectric and magnetic properties have been investigated.

2 Experimental Detail

The NF precursor was prepared form of nickel chloride ($NiCl_2.6H_2O$), iron chloride ($FeCl_3$), and KOH as the starting materials. These chlorides of nickel and iron were dissolved in mixture of ethanol and distilled water and subjected to stirring at room temperature for homogenous mixing for 2 h. The *p*H was adjusted to 13 by the addition of mineralizer KOH with stirring. The final solution was poured into teflon lined steel autoclave which was kept for heating in programmed furnace at 180°C for 48 h. The resultant material was washed several times with ethanol water mixture for purification and then dried at 80°C for 8 h in an oven. Similarly, for NZF, the starting materials are nickel chloride, iron chloride and zinc chloride ($ZnCl_2.6H_2O$), and for NZF/SF, additionally, strontium chloride was used. The procedure of synthesis is similar as used in the case of NF. The crystalline structure was analyzed by X-ray diffraction (XRD) by using X'Pert PRO PANalytical system and microstructure by transmission electron microscopy (TEM) by using HITACHI H-7500. Magnetization was measured at room temperature using Lakeshore 7304 vibrating sample magnetometer. The room temperature dielectric measurement was performed on NF, NZF and NZF/SF sample with frequency varying from 20 Hz to 120 MHz using Precision Impedance analyzer (Wayne Kerr 6500B).

3 Results and Discussion

Figure 1 shows the XRD pattern of NF, NZF and NZF/SF nanostructures synthesized by hydrothermal method at 180°C/48 h. In all NF and NZF, the major Bragg's peaks can be indexed using JCPDS data for cubic spinel phase with Miller indices (220), (311), (222), (400), (331), (422) and (511) are observed with diffraction angle at 2θ = 30.66°, 35.98°, 37.57°, 43.63°, 49.69°, 54.01° and 57.57°. However, the SF of composite NZF/SF, the orthorhombic phase of $SrFe_2O_4$ ferrites with Miller indices (121), (041), (141), (240), (002), (241), (102), (311), (202), (341), (400), (280), (290), (450), (223) and (520) are observed with diffraction angle at 2θ = 22.18°, 25.57°, 27.26°, 28.60°, 32.12°, 33.57°, 34.78°, 35.98°, 40.85°, 42.54°, 43.63°, 45.69°, 50.54°, 52.12°, 55.87°

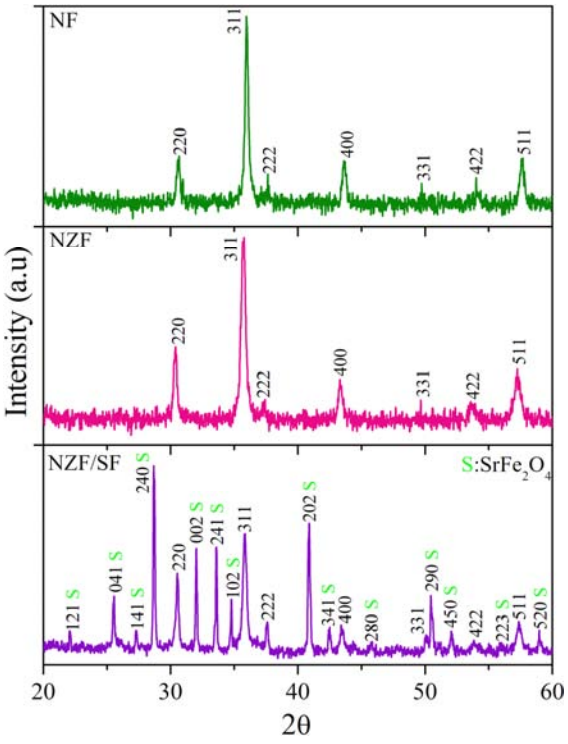

Fig.1 — XRD pattern of NF, NZF and NZF/SF nanostructure with hydrothermal conditions of 180°C/48 h

Table 1 — Values of lattice constant a, diameter (d), length (l), saturation magnetization (M_s), remanent magnetization (M_r), coercive field (H_c) and dielectric constant (ε_r) of NF, NZF and NZF/SF nanostructures

Sample	a (Å)	d (nm)	l (nm)	M_s (emu/g)	M_r (emu/g)	H_c(Oe)	e_r (10 MHz)
NF	8.403	19	-	35.78	2.01	26.13	60
NZF	8.417	23	325	54.89	3.03	33.86	91
NZF/SF	8.421/8.027	6	>160	52.36	41.41	203.89	125

and 59.15° are well matched with JCPDS data collected in the reported work[12]. The values of lattice constant a(Å) for cubic NF, NZF and orthorhombic SF ferrite are given in Table 1. The broadening of the full width at half maxima of the diffraction peaks indicates the formation of nanocrystalline products. Figures (2-4) show the TEM images at different magnification of NF, NZF and NZF/SF composite, respectively. As shown in Fig. 2, the NF is the product which consists of nanoparticles of very small size having cubic like faces of average diameter 19 nm. However, Figs. 3 and 4 show the nanowires like structures which consist of large number of nanowires in TEM images. The observed average diameter of wire is ~23 and 6 nm, and length 325 and 160 nm, respectively, for NZF and NZF/SF.

The growth mechanism in the formation of nanoparticles and nanowires of NF, NZF and NZF/SF by hydrothermal reactions tracks a liquid nucleation system as shown in Fig. 5. The principle involved chemical kinetics, theories of chemical equilibrium, and thermodynamic properties of water systems under hydrothermal conditions. Still a lot of work is needed to be done to explain mechanism under hydrothermal conditions. Few researchers have proposed dissolution-precipitation process by mechanism[13] on the basis of small crystalline nuclei in a suspension which is supersaturated and then it is monitored by crystal growth, in which the bigger particles will grow at the cost of the small ones owing to the energy difference between large particles and the smaller particles[14]. The ethanol water mixture 70:30 is used as a solvent[2]. Ethanol co-ordinates with metal ions and its solution with water make hydrothermal conditions optimum for the preparation and growth of particles. Homogenous mixture of solution of metal chlorides when interacts with OH^- ions of KOH at pH 13 behave differently. In the case of NF, Ni when reacts with OH^- forms $Ni(OH)_2$ readily undergoes oxidation to Ni oxy-hydroxide, NiOH, in combination with a reduction reaction, often of a metal hydride is given as:

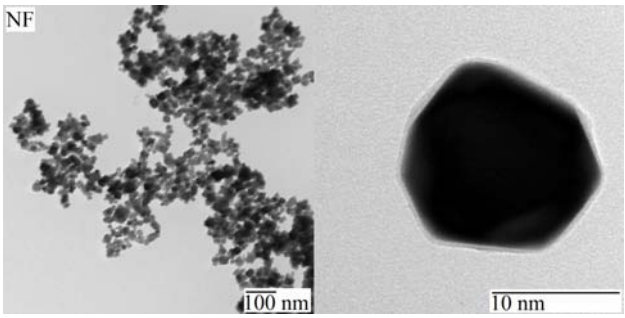

Fig. 2 — TEM images of SF nanoparticles

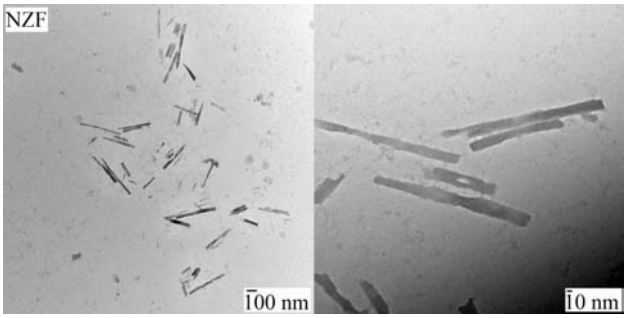

Fig. 3 — TEM images of NZF nanowires

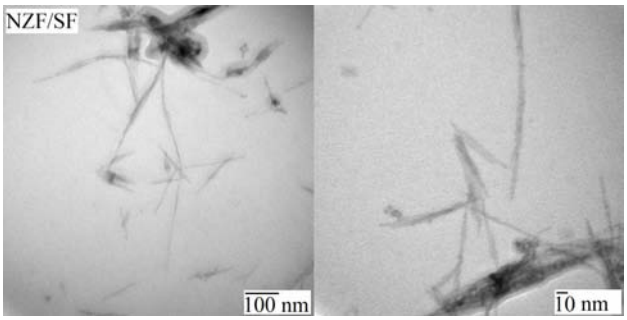

Fig. 4 — TEM images of NZF/SF nanowires

$$Ni(OH)_2+OH^- \rightarrow NiOH+H_2O+e^- \quad \ldots(1)$$

$$MH+OH^- \rightarrow M(metal)+H_2O+e^- \quad \ldots(2)$$

These reactions confirm no aggregation of particles in case of Ni– OH^- ion interactions, probably due to smaller ionic radius and surface free energy difference

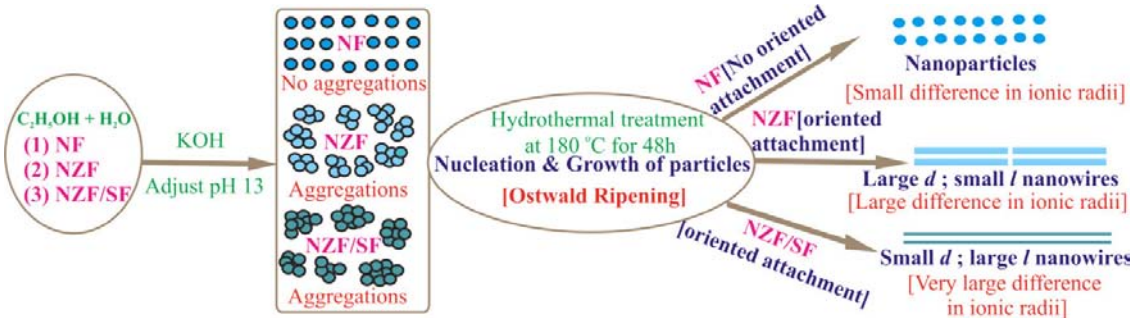

Fig. 5 — Crystal growth mechanism of NF, NZF and NZF/SF nanostructure

among ions. Whereas in case of NZF, Zn when comes in contact with OH^- forms aggregates, given as:

$$Zn^{2+}+2OH^-\rightarrow Zn(OH)_2 \quad \ldots(3)$$

$$Zn(OH)_2+2OH^-\rightarrow [Zn(OH)_4]^{2-} \quad \ldots(4)$$

Eq. (4) leads to chain like aggregates, this approach may be attributed to large ionic radius and surface free energy difference among precursors. The KOH will react with strontium chloride SrCl in a double displacement reaction. The balanced equation for this reaction is given as:

$$2KOH+SrCl_2\rightarrow Sr(OH)_2+2KCl \quad \ldots(5)$$

Aggregation is also observed in NZF/SF, when Sr in contact with OH^- ions. This aggregation can be attributed to larger ionic radius and surface free energy of Sr, leading to growth of particles. The ionic radii of Ni^{2+}, Zn^{2+}, Sr^{2+}, Fe^{2+} and Fe^{3+} are 0.83, 0.88, 0.132, 0.77 and 0.69 Å, respectively. On subjection to hydrothermal treatment, nucleation and growth of particles began which result into self-assembly, Ostwald[15] ripening takes place. In the case of NF, the crystal growth is splitting into nanoparticles and no oriental attachment because of Ni inactivity in formation of aggregates with OH^- ions. Thick wire formation is observed in NZF, which could be attributed to aggregation of Zn with OH^- ions. Oriental attachment in one crystallographic direction has led to their formation of thick wires. In NZF/SF, the thin nanowires have been formed, which is expected that there had been further splitting once they formed thick wires. The formation of thin wires is endorsed probably due to addition of one crystallographic plane by reason of steric hindrance on others.

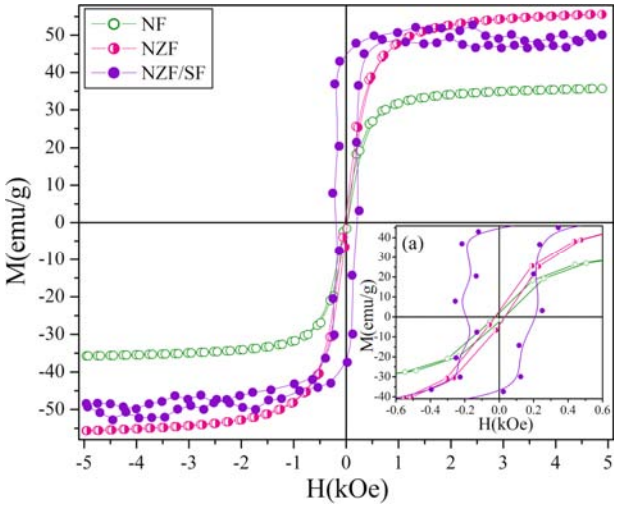

Fig. 6 — *M-H* hysteresis curves of NF, NZF and NZF/SF nanostructure. Inset (a) show the value of H_c

Figure 6 shows the ferromagnetic behaviour of NF, NZF and NZF/SF ferrites by measuring M-H hysteresis at room temperature. The values of saturation magnetization (M_s) are 35.78, 54.89 and 52.36 emu/g, remanent magnetization (M_r) 2.01, 3.03 and 41.41 emu/g, and coercive field (H_c) 26.13, 33.86 and 203.89 Oe, respectively, for NF, NZF and NZF/SF. The magnetic moment per formula unit in Bohr magneton (μ_B) was calculated using following relation[16] given as :

$$\mu_B = \frac{M \times M_s}{5585} \quad \ldots(6)$$

where M is the molecular weight of the sample, M_s is the saturation magnetization in emu/g. The calculated values of μ_B given in Eq. (6) are 3.601, 5.551 and 10.832, respectively, for NF, NZF and NZF/SF. According to Neel's two sub-lattices model of ferrimagnetism magnetic moment[16] can be expressed as:

$$n_B = M_B(x) - M_A(x) \quad \ldots(7)$$

where n_B is magnetic moment, $M_B(x)$ is magnetic moment of B site and $M_A(x)$ is magnetic moment of A site. In case of $NiFe_2O_4$, the value of magnetic moment exists due to distribution of Fe^{3+} ion on tetrahedral sites (A) and presence of Ni^{2+} and Fe^{3+} ions on octahedral (B) sites. In the $Ni_{0.6}Zn_{0.4}Fe_2O_4$, Zn^{2+} ions displace few of Fe^{3+} ions from tetrahedral (A) sites to octahedral (B) sites leading to overall increase in magnetic moment value. The calculated value of n_B is 2.43 and 5.24 for NF and NZF. However, the combined magnetic moment of composite phase NZF/SF is 10.41. The anisotropy constant (K) was calculated using the following relation[16]:

$$H_c = \frac{0.96 \times K}{M_s} \quad \ldots(8)$$

The values of K are 973.89, 1936.02 and 11120.51, respectively, for NF, NZF and NZF/SF.

The magnetic properties of NZF/SF nanowires are completely different. The hysteresis loops are two-step processes, typical of the exchange-spring regime. They show positive nucleation fields which is a peculiar prediction of a micro-magnetic model developed for perpendicular bilayers where the shape anisotropy contribution is also taken into account[17]. The overlap between the recoil curves and the main loop shows that the demagnetization process was perfectly reversible from the soft phase nucleation field down to the hard phase reversal field. In the low magnetizing field, the H_c and M_r show the loop as rectangular shaped indicating the strong coupling between hard and soft phases which leads to a magnetization reversal.

The dielectric constant (ε_r) and loss ($\tan\delta$) measurements in the frequency range 100 Hz-1 MHz and 1 MHz-120 MHz, are shown in Fig. 7 and 7(a), respectively. It is seen that the value of ε_r decreases with increasing frequency and at further higher frequencies it becomes slight variable. At lower frequency, the dispersion in dielectric constant is due to interfacial polarization. Due to rotational displacements at higher frequencies of the dipoles which result in the orientational polarization, dispersion in dielectric constant becomes small and approaches a nearly frequency independent response. The observed behaviour of the dielectric dispersion

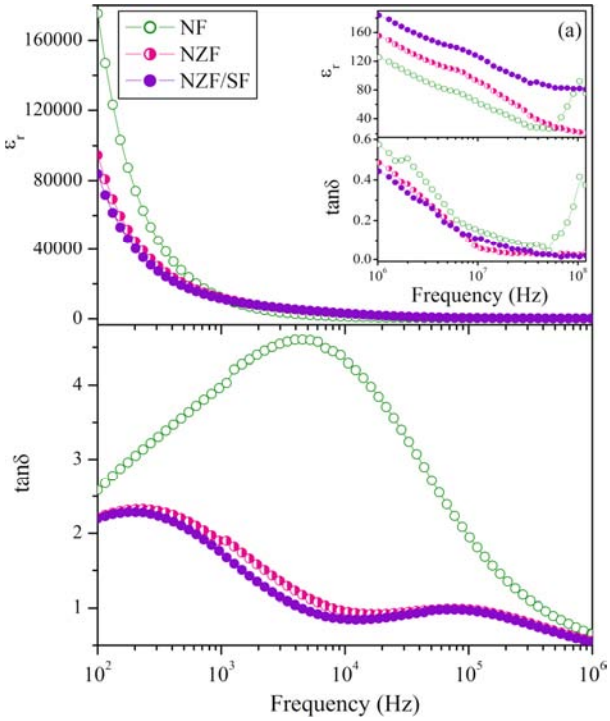

Fig. 7 — Frequency dependent relative permittivity (ε_r) and loss ($\tan\delta$) of NF, NZF and NZF/SF nanostructure. Inset (a) shows values at higher frequency region (1 MHz-120 MHz)

can be explained on the basis of Koops theory[18] and Maxwell-Wagner interfacial type of polarization[19]. In this model, a ferrite material is assumed to consist of well-conducting grains separated by less conducting grain boundaries. The electrons reach the grain boundary through hopping and if the resistance of the grain boundaries is high enough, electrons pile up at the grain boundaries and produce polarization. However, as the frequency of the applied field is increased, the electrons reverse their direction of motion more often. This decreases the probability of electrons reaching the grain boundary and as a result the polarization decreases. In the present case, all the grains are nano size whereas the large surface boundaries are the region of high resistance. This can reduce the interfacial polarization and hence improve the frequency dependent polarization process. A similar behaviour is involved in the case of loss factor.

With the addition of Zn and Sr in $NiFe_2O_4$, the dispersion in dielectric constant is observed up to frequency of 120 MHz. However, in case of pure NF, a resonance curve is observed in both frequency dependent ε_r and loss $\tan\delta$ nearly 60 MHz. This type of behaviour depends and also explained on the basis

of higher resistivity contributed by the nanostructure. The value of dielectric constant measured at 10 MHz is 60, 91 and 125, respectively, for NF, NZF and NZF/SF. The higher value of ε_r in the case of NZF and NZF/SF depends upon the types of nanostructure, i.e., nanoparticles in NF and nanowires in NZF and NZF/SF (large surface to volume ratio in nanowires than nanoparticles). The enhancement in polarization is adopted by an axial polarization[20] (the preferred polarization direction dictated by geometry). In 1D nanostructure, long range interaction is truncated due to the lack of periodicity and short range one is significantly modified near the surface boundary. However, Eliseev *et al*[21]. reported that the compressive stress induced by surface curvature would produce an effective tensile in the length direction of nanowires. The theoretical deductions by first-principles calculation responsible for the surface compressive stress caused by 1D confinement produces an effective tensile in the length direction in nanowires and then leads to a big off-center displacements that enhances the polarization. The near-surface depolarizing effects, which are mainly caused by the surface atomic relaxation, associated with finite thickness of wires are strong in low-dimensional structures, which cause, decrease of polarization than bulk[22] considerably.

4 Conclusions

The NF, NZF and NZF/SF ferrite were prepared by hydrothermal synthesis route. The growth mechanism in the formation of nanoparticles of NF and nanowires in NZF and NZF/SF is explained on the basis of aggregation of metal with OH^- ions by larger surface energy and ionic radii difference involves oriented attachment due to Ostwald ripening process during hydrothermal treatment. The XRD analysis results the formation of spinel phase of NF and NZF, and orthorhombic of SF ferrite. The TEM images results in nanoparticles of NF of average size is 19 nm. However, the nanowires of average diameter are ~ 23 and 6 nm, and length 325 and 160 nm, respectively, for NZF and NZF/SF. The values of M_s are 35.78, 54.89 and 52.36 emu/g, M_r are 2.01, 3.03 and 41.41 emu/g, and H_c are 26.13, 33.86 and 203.89 Oe, respectively, measured for NF, NZF and NZF/SF. At frequency of 10 MHz, the values of dielectric constant are 60, 91 and 125, respectively, measured for NF, NZF and NZF/SF. The improvement in dielectric polarization and the values observed at higher frequency are explained on the basis of size dependent nanostructures. The compressive stress induced by surface curvature of nanowire results in an effective tensile along the length direction leads to a large off-center displacement which enhances the polarization.

References

1 Ma X D, Nakagawa T, Takagi Y, Przybylski M, Leibsle F M & Yokoyama T, *Phys Rev B,* 78 (2008) 104420.
2 Kaur J, Negi N S, Kotnala R K & Verma K C, *J Sol-Gel Sci Technol,* 65 (2013) 411.
3 Chen M, Pica T, Jiang Y B, Li P, Yano K, Liu J P, Datye A K & Fan H, *J Am Chem Soc,* 129 (2007) 6348.
4 Kanagaraj M, Sathishkumar P, Selvan G K, Kokila I P & Arumugam S, *Indian J Pure & Appl Phys*, 52 (2014) 124.
5 Verma K C, Singh V P, Ram M, Shah J & Kotnala R K, *J Magn Magn Mater,* 323 (2011) 3271.
6 Mohanty V, Cheruku R, Vijayn L & Govindaraj G, *Indian J Pure & Appl Phys,* 51 (2013) 381
7 Thomas J J, Shinde A B, Krishna P S R & Kalarikkal N, *J Alloy Compd,* 546 (2013) 77.
8 Singh S, Ralhan N K, Kotnala R K & Verma K C, *Indian J Pure & Appl Phys,* 50 (2012) 739.
9 Singh S, Singh M, Ralhan N K, Kotnala R K & Verma K C, *Adv Sci Engg Med*, 6 (2014) 688.
10 Verma K C & Kotnala R K, *J Nanopart Res,* 13 (2011) 4437.
11 Suess D, Schrefl T, Kirschner R M D, Dorfbauer F, Hrkac G & Fidler J, *J Magn Magn Mater,* 290 (2005) 551.
12 Berthet P, Berthon J, Heger G & Revcolevschi A, *Mat Res Bull*, 27 (1992) 919.
13 Eckert J O, Hung-Houston C C, Gersten B L, Lencka M M & Riman, *J Am Ceram Soc,* 79 (1996) 2929.
14 Mullin J W, *Crystallization* (3rd Edition), Butterworth-Heinemann, Stoneham, MA, 1997.
15 Ostwald W F, *Phys Chem*, 22 (1897) 289.
16 Sharma R & Singhal S, *Physica B*, 414 (2013) 83.
17 Casoli F, Nasi L, Albertini F, Fabbrici S, Bocchi C, Germini F, Luches P, Rota A & Valeri S, *J Appl Phys,* 103 (2008) 043912.
18 Koops C J, *Phys Rev,* 83 (1951) 1520.
19 Wagner K W, *Ann Phys,* 40 (1913) 817.
20 Pilania G, Alpay S P & Ramprasad R, *Phys Rev B,* 80 (2009) 014113.
21 Eliseev E A, Morozovska A N, Glinchuk M D & Blinc R, *Phys Rev B*, 79 (2009) 165433.
22 Junquera J & Ghosez P, *Nature (London)*, 422 (2003) 506.